PCCP

Tuning the melting point of selected ionic liquids through adjustment of the cation's dipole moment.

Journal:	*Physical Chemistry Chemical Physics*
Manuscript ID	CP-ART-03-2020-001214.R2
Article Type:	Paper
Date Submitted by the Author:	07-May-2020
Complete List of Authors:	Rabideau, Brooks; The University of South Alabama Soltani, Mohammad; The University of South Alabama Parker, Rome; The University of South Alabama Siu, Benjamin; The University of South Alabama Salter, Edward; The University of South Alabama Wierzbicki, Andrzej; The University of South Alabama West, Kevin; The University of South Alabama Davis, Jr, James; The University of South Alabama

Cite this: DOI: 00.0000/xxxxxxxxxx

Tuning the melting point of selected ionic liquids through adjustment of the cation's dipole moment.†

Brooks D. Rabideau,*[a] Mohammad Soltani,[b] Rome A. Parker,[a], Benjamin Siu,[a] E. Alan Salter,[b] Andrzej Wierzbicki,[b] Kevin N. West,[a] and James H. Davis Jr.*[b]

Received Date
Accepted Date

DOI: 00.0000/xxxxxxxxxx

In previous work with thermally robust salts [Cassity *et al., PCCP*, 2017, **19**, 31560] it was noted that an increase in the dipole moment of the cation generally led to a decrease in the melting point. Molecular dynamics simulations of the liquid state revealed that an increased dipole moment reduces cation-cation repulsions through dipole-dipole alignment. This was believed to reduce the liquid phase enthalpy, which would tend to lower the melting point of the IL. In this work we further test this principle by replacing hydrogen atoms with fluorine atoms at selected positions within the cation. This allows us to alter the electrostatics of the cation without substantially affecting the sterics. Furthermore, the strength of the dipole moment can be controlled by choosing different positions within the cation for replacement. We studied variants of four different parent cations paired with bistriflimide and determined their melting points, and enthalpies and entropies of fusion through DSC experiments. The decreases in the melting point were determined to be enthalpically driven. We found that the dipole moment of the cation, as determined by quantum chemical calculations, is inversely correlated with the melting point of the given compound. Molecular dynamics simulations of the crystalline and solid states of two isomers showed differences in their enthalpies of fusion that closely matched those seen experimentally. Moreover, this reduction in the enthalpy of fusion was determined to be caused by an increase in the enthalpy of the crystalline state. We provide evidence that dipole-dipole interactions between cations leads to the formation of cationic domains in the crystalline state. These cationic associations partially block favourable cation–anion interactions, which are recovered upon melting. If, however, the dipole-dipole interactions between cations is too strong they have a tendency to form glasses. This study provides a design rule for lowering the melting point of structurally similar ILs by altering their dipole moment.

1 Introduction

The melting point of a compound is one of its most defining properties, often dictating its suitability for a given application. For this reason, and likely in an attempt to distinguish research from that of molten salts, ionic liquids (ILs) somehow came to refer to salts melting at or below 100 °C. Most inorganic salts, however, melt many hundreds of degrees higher than this relatively arbitrary definition, leaving an enormous gap between these two distinctions. In reality, a spectrum of melting points exists as attested by the many organic salts that melt somewhere in-between. These mesothermal salts still possess the same tunable nature, structure, and other desired properties shared by ILs. Therefore, it makes more sense that we forgo this arbitrary definition and refer to these compounds as *mesothermal ionic liquids*.[1]

These mesothermal ILs have great promise for applications as heat transfer fluids, lubricants for extreme conditions, solvents for biomass pretreatments, and as catalysts for high temperature reactions. Recently, a series of peraryl phosphonium and sulfonium salts have been identified as having long-term thermal stability that significantly increases their suitability for these important applications.[2] Only a few of these compounds fit the traditional definition of an IL while many were found to have melting points between 100–200 °C. To reduce energy expenditures and extend the range of applicability of these compounds it is desirable to drive their melting points down, creating a wider liquidus range.

[a] *Department of Chemical & Biomolecular Engineering, The University of South Alabama, Mobile, Alabama 36688, USA. Fax: (251) 461-1485; Tel: (251) 460-7147; E-mail: brabideau@southalabama.edu*
[b] *Department of Chemistry, The University of South Alabama, Mobile, Alabama 36688, USA. E-mail: jdavis@southalabama.edu*
* *Corresponding authors*

† Electronic Supplementary Information (ESI) available: Details on the synthesis, NMR of all compounds, single crystal structures (CCDC Deposition 1986291-1986294), and typical DSC scans of the compounds. See DOI: 00.0000/00000000.

Ways to increase the liquidus range of pure compounds through structural modification generally focus on either maximizing the compound's ability to form supercooled liquids and glasses[3] or by directly driving the melting point down. One such study concerning the former showed that small symmetric molecules that form multiple hydrogen bonds were good glass formers.[4] Here, multiple strong, directional interactions work to thwart crystallization. Recently it was shown that IL cations possessing the ability to form hydrogen bonds could overcome the strong electrostatic repulsion to form cationic clusters.[5] Moreover, the formation of cationic clusters was shown to affect the properties of ILs, notably leading to the formation of glasses. Quantum–based calculations showed that hydrogen bonding can be sufficiently strong to stabilize these cationic clusters, overcoming the strong electrostatic repulsions.[6] In another study, it was shown that, given the structure of the crystal lattice, one can use first-principle simulations to reproduce the melting point trends of different IL variants.[7] Methods focused on driving the melting point down are challenging however, because it remains difficult to predict the crystalline state of a compound from chemical structure alone. Due to this difficulty many studies have resorted to large-scale screening of structurally similar compounds and quantitative structure–property relationships (QSPR).[8] Perhaps the simplest guideline is Carnelley's rule stating that asymmetric molecules generally have lower melting points than symmetric molecules.[9] Another well–known principle is delocalization of charges within the ions.[10] This was recently illustrated for a tetralkylphosphonium salt having a melting point 60 °C lower than the equivalent tetraalkylammonium salt despite the two having isomorphous structures.[11] In this case, an increase in charge delocalization and polarization within the cation led to a weakening of the IL network. In a study looking at lipid–inspired ionic liquids it was found that the addition of side chain unsaturations could significantly depress the melting point.[12] Furthermore, it was found that this could be achieved through the incorporation of ether, thioether,[13,14] or cyclopropyl moeities[15] to the side chain or even through the addition of two lipid-like aliphatic tails.[16] Additionally, it was found that the incorporation of both aromatic and aliphatic substituents at the imidazolium ring, referred to as TAAILS, allows for the more precise tuning of IL properties.[17]

Due to the complex interactions present in ILs, similar compounds can have significantly different melting points for reasons that are not entirely understood. Hydrogen bonds are generally thought of as having a stabilizing effect on molecular structures. Surprisingly however, methylation at the C2 position of 1,3-dialkylimidazolium based ionic liquids, which removes the primary mode for hydrogen bonding leads to an increase in both melting point and viscosity.[18–20] This was hypothesized to be due to a loss in entropy,[21,22] however it was later reasoned that his alone could not explain this behaviour.[23] Additional studies on imidazolium-based ILs showed that strong, localized, and directional hydrogen bonds can decrease melting points and viscosities of these compounds.[24,25] This was said to occur due to the introduction defects into the Coulomb networks of ILs through these localized interactions. It still remains unclear to what extent this concept translates to other classes of ionic liquids and how this affects the molecular driving forces. The lack of more comprehensive guidelines for the design of new ILs with a larger liquidus range effectively hinders the discovery of new and important compounds. If we fully understood how the structure of an IL is tied to its melting point this would significantly help in the discovery of new ILs and their integration in industrial processes.

In previous work with perarylphosphonium-based ILs it was found that the addition of asymmetric moieties, and variations in the substituent type and position had a large effect on the melting point.[26] Molecular dynamics simulations of the liquid state showed that those compounds with low melting points had cations that tended to align. This was attributed to their higher dipole moments, which was substantiated through correlations between quantum-based calculations of the dipole moment and the experimental melting point. It was believed that these cation–cation alignments in the liquid state lowered the repulsions between these like charges in the liquid state, lowering the enthalpy of fusion. In this work, however, we find that cation–cation alignments are much stronger in the crystalline state. These alignments thwart more favourable interactions, raising the enthalpy of the solid state, another way of lowering the enthalpy of fusion.

In this work we test the idea of altering the dipole moment of the cation, effectively introducing strong, directional interactions,[24,25] as a means of lowering the melting point by systematically replacing hydrogen atoms with fluorine atoms at specific locations throughout the cation. Fluorine's use as an isostere for hydrogen is a well-established practice[27] and allows one to alter the electrostatic charge distribution throughout the cation without significantly affecting the sterics. Thus this provides us with a way of uniquely adjusting the dipole moment of an IL cation. This was done with four different cation classes: perarylphosphonium and perarylsulfonium, piperidinium, and imidazolium (see Figure 1) all paired with the anion bistriflimide.

We used differential scanning calorimetry (DSC) to precisely measure the melting points of these compounds. Independently, we used quantum–based calculations to determine the dipole moments of each of the cations. We find that cations with higher dipole moments generally have lower melting points. Molecular dynamics (MD) simulations of the solid and liquid states were in close agreement with the experimentally determined thermodynamic properties. Furthermore, we find that higher dipole moments coax the cations to assemble into cationic domains in the crystalline state. These cation–cation associations raise the free energy of the crystalline state by blocking some of the favourable cation–anion interactions. Upon melting, these favourable interactions are recovered resulting in a lower enthalpy of fusion, which lowers the melting point.

2 Methods

2.1 Materials and Representative Synthesis

Preparation of the ionic liquids in Figure 1 and corresponding Table 1 followed established protocols from earlier studies.[1,2,26,28–31] Further information regarding their synthesis and characterization as well as the NMR spectra of all of the compounds can be found in the ESI.

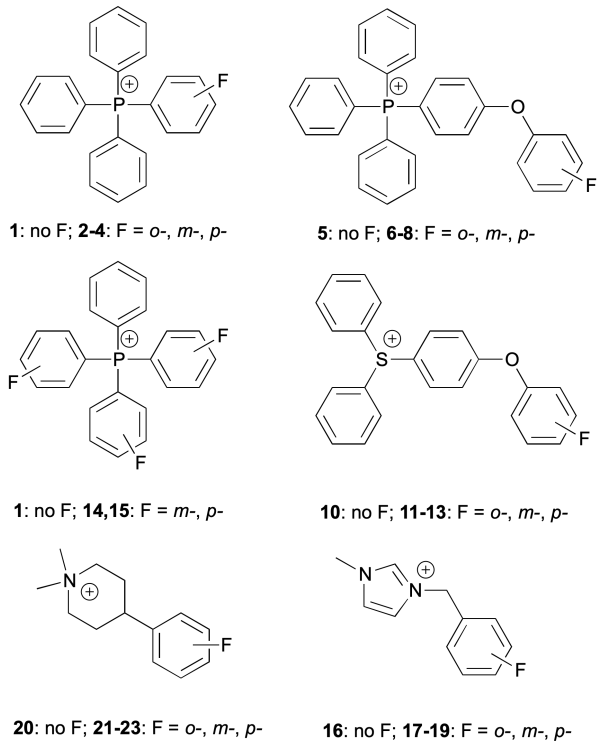

Fig. 1 Structures of the IL cations with variable fluorine position. The numbering corresponds to the entries in Table 1 and throughout the text. Numbering of the parent cations are given in parentheses.

The crystalline structure of several of the synthesized compounds that formed crystals were determined via single–crystal X-Ray diffraction. These details and the crystallographic information files of these compounds are given in the ESI.

2.2 Differential Scanning Calorimetry

At the melting point, equilibrium exists between the solid and liquid phases and the change in Gibbs free energy is zero:

$$\Delta G_{fus} = 0 = \Delta H_{fus} - T_m \Delta S_{fus}, \quad (1)$$

where ΔH_{fus} is the enthalpy of fusion, T_m is the melting point, and ΔS_{fus} is the enthalpy of fusion. Thus the melting point is determined as a delicate balance between the enthalpy and entropy of fusion:

$$T_m = \frac{\Delta H_{fus}}{\Delta S_{fus}}. \quad (2)$$

Note that decreases in the ΔH_{fus} and increases in ΔS_{fus} both drive the melting point down.

Sample melting points, glass transition temperature, and enthalpies of fusion were measured on TA Instruments Q2000 Differential Scanning Calorimeter (DSC). The entropies of fusion were calculated as the enthalpy of fusion divided by melting point in absolute temperature. Melting points are reported as the transition from the solid (crystalline/ordered) to the isotropic liquid and glass transitions are reported as the transition from the amorphous (disordered) solid to the isotropic liquid, distinguished by both the magnitude of the enthalpy for the transition and the shape of the DSC curve. For each experiment, 1-20 mg of the sample was loaded into an open DSC pan and heated to 110 °C for 10-30 minutes to remove any water absorbed from the environment, residual solvent, or volatile contaminants from synthesis. The samples were then cooled to -80 °C, equilibrated for 2 minutes and then heated at a ramp rate of 10 °C/minute to the upper temperature of each run, typically 300 °C. Melting points are reported as the melting onset temperature as determined by the software and glass transitions are reported as the midpoint of the transition. All measurements were carried out under UHP nitrogen flowing over the sample cell at 50 mL/minute. Reported values are the average of at least three measurements and the standard uncertainty is reported as the standard deviation of the mean.

2.3 Quantum-Based Calculations

The isolated cations were optimized (gas phase) using the B3LYP density functional method and the 6-31G* basis set as implemented in Gaussian16 (Gaussian, Inc., Wallingford, USA).[32] All structures were confirmed as stable by computing analytic vibrational frequencies, then reoptimized using the 6-311+G(d,p) basis set; dipole moments were concurrently computed with the origin placed at the center of nuclear charge (as is the default). We note that the gas-phase optimized cations used for the dipole calculations adopted nearly identical conformations as the cations in the crystal structures. Of the three crystal structures we obtained, which had conformational flexibility, two had exactly one unique cation per structure ($Z' = 1$) and the other had two unique cations per structure ($Z' = 2$). The only perceptible differences between the gas-phase optimized cations and the cations in the crystal structures are limited to phenoxyphenyl torsion angles that vary by less than 20° as well as 180° rotations of the terminal fluorophenyl groups caused by disorder. The latter is discussed in the context of our findings, where it will be shown that this principle holds true under these rotations. Isodensity electrostatic potential energy maps (elstats) were generated by Spartan '08 (Wavefunction, Inc., Irvine, CA) in follow-up single-point calculations.

2.4 MD Simulations

Ionic liquid cations and anions were modeled using the General AMBER Force Field (GAFF).[33] Electrostatic potentials were derived using the Hartree-Fock model and the 6-31G* basis set in Gaussian09 (v.09, revision E.01, Gaussian, Inc., Wallingford, USA).[32] Point charges for the GAFF models were fit from these electrostatic potentials using the restrained electrostatic procedure (RESP).[34] Additionally, the partial charges were scaled by 80% since it was shown in previous works that doing so with GAFF, one can accurately predict the thermodynamic and transport properties for ILs.[35] This scaling was applied equally to the partial charges of atoms in each respective ion.

Molecular dynamics (MD) simulations were performed with LAMMPS[36] using periodic boundary conditions and a short-range cutoff of 12 Å. Long-range electrostatics were included using the

particle-particle particle-mesh (pppm) method with an accuracy of 1×10^{-4}.[37] Initial configurations of the solid phase were created by replicating the primitive cell into a 3x3x3 supercell containing 216 ion pairs. These configurations were then slowly heated from 1 K to 400 K over 100 ps in the *NPT* ensemble at 1 atm using a thermostat of 100 fs and a barostat of 1000 fs. The production run consisted of a 2 ns long simulation in the *NPT* ensemble at 400 K and 1 atm using the same thermostat and barostat. Initial configurations for the liquid phase simulations were created by placing 210 ion pairs in a 70 Å $\times$70 Å $\times$70 Å simulation box using PACKMOL.[38] A 21-step compression and relaxation scheme was then used to achieve a stable liquid density.[39] Finally, the production run consisted of a 20 ns long simulation in the *NPT* ensemble at 400 K and 1 atm using the same thermostat and barostat as the solid phase simulation. Thermodynamic data was output every 100 fs and trajectories output every 20 ps.

3 Results and Discussion

3.1 Thermodynamic Analysis

3.1.1 General Trends

In general, appending a fluorine onto a phenyl ring appended to the cation of an ionic liquid increases the dipole moment of the cation. This can be seen in Figure 2, which shows the electrostatic potential of one of the homologous series of cations with variations in the fluorine position. Generally, this increase in the dipole moment of the cation decreases the enthalpy of fusion significantly and decreases the entropy of fusion modestly, resulting in a decrease in the melting point. The effects observed upon substituting the fluorine in the specific *ortho*, *meta* or *para* positions on the ring are more complex and specific to the homologous series. A summary of these results is given in Table 1. Note that the melting points of parent compounds **1**, **5**, **9**, and **10** were taken from our earlier works.[26,29] The dipole moments of compounds **1**, **5** were also reported earlier,[26] however the structures were re-optimized using a different basis set and the dipole moments re-calculated. In the sections that follow, results from quantum and molecular dynamic calculations provide insights into the trends observed below.

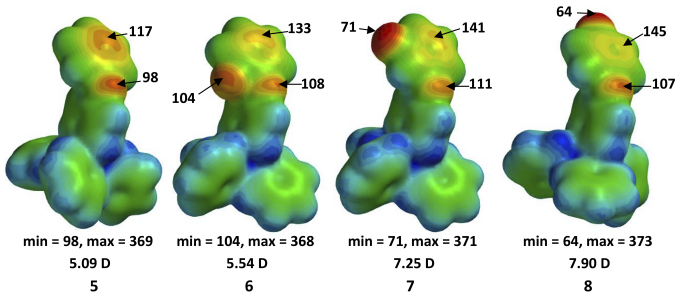

Fig. 2 From left to right: electrostatic potential energy maps of cations **5**, **6**, **7**, and **8**. These correspond to the parent cation and the cations with *o*, *m*, and *p*–linked fluorines, respectively. Common elstat range: 64 (red) to 373 (blue) kJ/mol.

3.1.2 $(Ph)_3$P-*x*-F-Ph^+ Series 1-4

As a fluorine atom is substituted onto a single phenyl ring of the cation of tetraphenylphosphonium bistriflimide (**1**) to give compounds **2**-**4**, the ΔH_{fus} decreases for all three compounds. The ΔH_{fus} decrease is most pronounced (40%) for **2**, the *ortho* substituted compound, with the ΔH_{fus} of the *meta* (**3**) and *para* (**4**) substituted compound decreasing 34% and 27% respectively. Similarly, the ΔS_{fus} also decreases for each compound in the same pattern: 39% for the *ortho* substituted, 29% for the *meta* substituted and 21% for the *para* substituted cation. For each species, the decrease in ΔH_{fus} is subtly larger than the decrease in ΔS_{fus} resulting in a melting point decrease relative to the unsubstituted salt. Because the decreases in the ΔH_{fus} and ΔS_{fus} for **2** nearly offset each other, the melting point of **2** is just slightly lower than that of **1**. Similarly, the substantially larger decreases in ΔH_{fus} relative to ΔS_{fus} in both **3** and **4** result in larger melting point decreases for these salts relative to **1**. In this simplest case, the melting point changes inversely with the dipole moment of the cation.

3.1.3 (*x*-F-Ph)$_3$P- Ph^+ Series 1,14-15

For species **14** and **15**, the comparator is again **1**. These salts are similar to **2**-**4**, however, rather than having one of the four phenyl rings replaced with a *meta* or *para*-fluorophenyl, three of the four rings have been replaced with the same fluorophenyl substituent, **14** being the tri(*m*-F-phenyl)phenylphosphonium and **15** being the tri(*p*-F-phenyl)phenylphosphonium. Note that tri(*o*-F-phenyl)phenylphosphonium was not synthesized due to unavailability of starting materials. For these two salts, the melting point difference from **1** is enthalpically driven, interestingly, in opposite directions. Compared to **1**, the ΔH_{fus} of **14** is 25% higher and the ΔS_{fus} is 19% higher, resulting in a melting point increase of 18 °C. However, when **15** is compared to **1**, the ΔH_{fus} of **15** is 51% lower and the ΔS_{fus} is 41% lower, resulting in a significant melting point decrease of 67 °C. Of note is that unlike the previous species, the dipole moment of **14** is larger than both **1** and **15**, even though it has a higher melting point. This is discussed in further detail in the sections below.

3.1.4 $(Ph)_3$P-*p*-POP-*x*-F^+ Series 5-8

The next series of salts (**5**-**8**) demonstrates the effect of substituting a fluorine atom on the outer phenyl ring of the *p*-phenoxyphenyl (POP) substituent on a triphenyl-*p*-phenoxyphenylphosphonium cation (**5**), again in the *ortho* (**6**), *meta* (**7**) and *para* (**8**) positions of the ring. For this series, the effects of the substitution on the ΔH_{fus} and ΔS_{fus} are more subtle, although the melting point changes are equally significant. When the fluorine atom is place in the *ortho* position (**6**), there is a 1% increase in ΔH_{fus} and a 3% decrease in ΔS_{fus} (relative to **5**). Even though these effects are small, they both serve to increase the melting point relative to **5**, an increase in T_m of 17 °C. Conversely, when the fluorine atom is place in the *meta* position (**7**) the ΔH_{fus} decreases by 13% and the ΔS_{fus} decreases by 5%, resulting in an enthalpy difference driven melting point decrease of 34 °C. For this series, the *para* substituted species (**8**) was observed to undergo a glass transition at 3 °C rather than a melt from an ordered

crystal to the isotropic liquid, thus its enthalpy and entropy of fusion cannot properly be compared with the other species. However, such a transition is indicative of the modification disrupting order and structure frustrating solid phase packing.

Also note that when comparing cation **7** relative to **6**, which are isomers, there is a 14% drop in ΔH_{fus} and only a 1% drop in ΔS_{fus}. The net result of this seemingly minor change in fluorine position from the *ortho* to *meta* position is a 50 °C drop in the melting point that is almost entirely enthalpy driven. In the following sections we will use these two cations as our base comparison for understanding the molecular–level driving forces of this large drop in melting point.

3.1.5 $(Ph)_2$S-*p*-POP-*x*-F^+ Series 9-13

This series is similar to the previous one in that it involves substituting a fluorine atom in the *ortho* (**11**), *meta* (**12**) or *para* (**13**) position of the outer ring of a POP substituent on a cation, in this case a sulfonium cation. The comparator for this series is the unsubstituted diphenyl-*p*-phenoxyphenylsulfonium cation (**10**) and the simplest peraryl species, triphenylsulfonium cation (**9**) is shown for context, each of these being examined in a previous study. In this series both the *ortho* (**12**) and *para* (**14**) fluoro substituted species exhibit glass transitions at similarly low temperatures, -21 °C and -16 °C, respectively, again indicative of frustrating solid phase organization and packing. The *meta* (**13**) substituted species exhibits a 15% decrease in ΔH_{fus} and a 13% decrease in ΔS_{fus}, resulting in an 8 °C decrease in melting point.

3.1.6 1-Me-3-*x*-F-Benzyl IM Series 16-19

Although this work was prompted by insights developed from studying the thermally robust phosphonium and sulfonium analogues above, a broader understanding of the effect of polarity and dipole moments on the thermodynamic properties of ionic liquids invites investigation of a more diverse set of compounds. To that end the following methyl benzyl imidazolium bistriflimide salts were also examined. Here the parent salt is 1-methyl-3-benzylimidazolium bistriflimide (**16**), with **17**-**19** being the *ortho*, *meta* or *para* fluorobenzyl substituted analogues, respectively. Unfortunately, three of the salts (**16**-**18**), exhibit a glass transition rather than a melting point, making systematic thermodynamic analysis of the thermodynamics of fusion of the species impossible. However, as noted earlier, several previous studies have shown that molecules capable of forming strong directional interactions increases their tendency to form glassy states, effectively interfering with the molecules ability to sample local minima necessary for crystallization. We believe that the protons on the imidazolium ring are sufficiently strong to interfere with crystallization in a similar manner as described in those earlier studies.

3.1.7 N,N-Dimethyl-4-(*x*-F-phenyl)piperidinum Series 20-23

Although analysis of the imidiazolium series above proved intractable due to observation of glass transitions rather than crystal to isotropic liquid transitions, analysis of the piperidinum series proved more instructive. Here the parent salt is N,N-dimethyl-4-phenylpiperidinium bistriflimide (**20**) and the substituted analogues (**21**-**23**) have a fluorine atom in the *ortho*, *meta* or *para* positions of the phenyl ring, respectively. In this series, the largest change in melting point is observed for the *ortho* substituted salt (**21**) which, when compared to **20**, has a melting point that is 28 °C lower driven by a ΔH_{fus} that is 20% lower than that of **20**, overcoming the smaller decrease in ΔS_{fus} of only 15%. Although **23** has a similar melting point decrease relative to **20** (25 °C lower) it is driven by smaller decreases in ΔH_{fus} and ΔS_{fus}, 10% and 3% respectively. The *meta*-fluoro substituted species (**22**) has a similar decrease in ΔS_{fus} (3% relative to **20**) as that of **23**, however, it exhibits a smaller decrease in ΔH_{fus} (8% relative to **20**), resulting in a smaller melting point decrease of only 18 °C.

3.2 Effect of the Dipole Moment

All of the cations in Table 1 with a parent cation that did not form a glass were analyzed and the results given in Figure 3. In this figure, the differences indicate the values of the fluorinated compound relative to that of the corresponding parent compound. In general, the figure shows that increasing the dipole moment of the cation leads to a drop in the melting point. Eight of the eleven compounds with data allowing for comparison showed a significant drop. The exceptions in this figure will addressed in a later section.

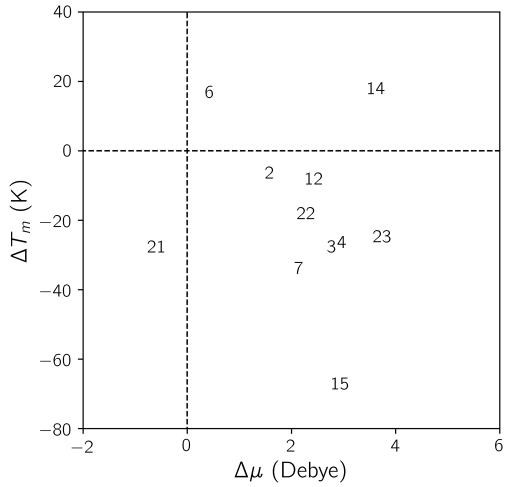

Fig. 3 The relation between the change in the dipole moments $\Delta\mu$ of the cations and the change in the melting point ΔT_m for selected cations in Table 1. The change is calculated as the value of the selected cation minus the value of the corresponding parent cation.

3.3 MD Simulations: A Comparison of Compounds 6 and 7

Cations **6** and **7** showed one of the largest differences in melting point among all of the isomers; a difference of over 50 °C. Interestingly, this large drop in melting point occurs from a seemingly minor change in the fluorine atom from the *ortho* to the *meta* position. In the next sections we compare these two compounds using insights gained from molecular dynamics simulations.

Table 1 Melting points, enthalpies and entropies of fusion of the salts. Uncertainties given are the standard deviation of the mean.

#	Cation	Dipole Moment (D)	T_m (°C)	$T_m \pm u_c$ (K)	$\Delta H_{fus} \pm u_c$ (kJ mol^{-1})	$\Delta S_{fus} \pm u_c$ (J mol^{-1} K^{-1})
1	PPh_4^+	0	135.0[c]	408.2 ±0.1	32.3 ±0.1	79.2 ±0.3
2	P(Ph)$_3$-*o*-F-Ph$^+$	1.60	128.5	401.7 ±0.3	19.3 ±0.1	48.1 ±0.2
3	P(Ph)$_3$-*m*-F-Ph$^+$	2.79	107.1	380.3 ±0.2	21.4 ±0.9	56.0 ±0.2
4	P(Ph)$_3$-*p*-F-Ph$^+$	2.98	108.5	381.7 ±0.1	23.7 ±0.2	62.2 ±0.4
5	P(Ph)$_3$-*p*-POP$^+$	5.09	102.1[c]	375.3 ±0.2	33.8 ±0.3	90.1 ±0.8
6	P(Ph)$_3$-Ph-*p*-(*o*-F-POP)$^+$	5.54	118.7	391.9 ±0.5	34.1 ±0.5	87.0 ±1.5
7	P(Ph)$_3$-Ph-*p*-(*m*-F-POP)$^+$	7.25	68.2	341.3 ±0.2	29.3 ±0.6	85.9 ±1.8
8	P(Ph)$_3$-Ph-*p*-(*p*-F-POP)$^+$	7.90	3.0*	276.1 ±0.5	– –	– –
9	SPh_3^+	0.27	92.4[d]	365.7 ±0.1	34.3 ±0.1	93.5 ±0.4
10	SPh$_2$-*p*-POP$^+$	6.00	62.7[d]	335.9 ±0.5	18.1 ±0.2	53.8 ±0.6
11	Ph$_2$S-*p*-(*o*-F-POP)$^+$	6.30	-21.4*	251.7 ±1.3	– –	– –
12	Ph$_2$S-*p*-(*m*-F-POP)$^+$	8.38	54.6	327.7 ±0.8	15.4 ±0.9	47 ±3
13	Ph$_2$S-*p*-(*p*-F-POP)$^+$	9.23	-16.3*	256.9 ±0.2	– –	– –
14	P(*m*-F-Ph)$_3$Ph$^+$	3.57	152.8	426.0 ±0.2	40.3 ±0.3	94.5 ±0.8
15	P(*p*-F-Ph)$_3$Ph$^+$	2.88	67.7	340.8 ±1.0	15.9 ±0.6	47 ±2
16	MBzIM$^+$	6.14	-55.2*	218.0 ±0.1	– –	– –
17	M-*o*-F-BzIM$^+$	6.58	-58.8*	214.3 ±0.1	– –	– –
18	M-*m*-F-BzIM$^+$	8.56	-60.8*	212.3 ±0.2	– –	– –
19	M-*p*-F-BzIM$^+$	9.31	47.7	320.8 ±0.1	31.1 ±0.1	96.8 ±0.3
20	DM-4-Ph-PIP$^+$	10.06	137.1	410.2 ±0.1	31.3 ±0.1	76.2 ±0.1
21	DM-4-(*o*-F-Ph)-PIP$^+$	9.40	109.3	382.4 ±0.2	24.9 ±0.1	65.0 ±0.3
22	DM-4-(*m*-F-Ph)-PIP$^+$	12.27	118.8	392.0 ±1.0	28.9 ±0.5	73.7 ±1.2
23	DM-4-(*p*-F-Ph)-PIP$^+$	13.73	112.0	385.2 ±0.1	28.4 ±0.2	73.6 ±0.5

* glass transition from amorphous solid to the isotropic liquid.

[c] taken from earlier work.[26]

[d] taken from earlier work.[29]

3.3.1 Thermodynamics

Simulations were performed for both the crystalline and liquid states of **6** and **7** at 400 K and 1 atm. The calculated enthalpies of fusion are given in Table 2 along with the thermodynamic properties obtained from DSC experiments. The bottom row of Table 2 shows the difference in each quantity between **6** and **7**. The calculated difference in the enthalpies of fusion ($\Delta\Delta H_{fus}$) is -4.9 kJ/mol, which nearly matches the experimentally determined value of -4.8 kJ/mol. As noted earlier, the DSC measurements that corresponded to a 50 °C drop in melting point between these two compounds was almost entirely driven by changes in ΔH_{fus}. Since this effect is accurately captured by the simulations, we now focus on understanding what changes in the molecular behaviour underly this drop in enthalpy.

The change in enthalpy ΔH can be further broken down into changes in energy ΔU and changes in the pressure-volume term $p\Delta V$. The changes in the energy can be further broken down into changes in pairwise interaction energies ΔU_{pair} and changes in molecular energies ΔU_{mol} (e.g. bonds, angles, dihedrals, impropers). The primary contribution to ΔH however, are the changes in the former, ΔU_{pair}. ΔU_{pair} can be further broken down into contributions between the cation-cation, cation-anion, anion-anion, and even between specified groups of atoms within these ions. This breakdown is given in Table 3. At the far right of Table 3, the overall drop in the enthalpy (-4.9 kJ/mol) is shown to roughly match the change in pairwise interaction energy of -6.7 kJ/mol. Moving left, the primary cause of this drop is shown to be a drop of -9.6 kJ/mol in the anion–cation (ANI–CAT) interaction energy. Continuing left, this drop in anion–cation energy is mostly a result of a drop in the anion-triphenylphosphonium (ANI-TRI) energy as opposed to the anion-phenoxyfluorophenyl (ANI-POP) energy. In a recent study it was shown that substitution of phenyl groups for hexyl groups in quaternary phosphonium cations significantly decreases hydrogen bonding through a reduction in conformational flexibility.[40] Thus, it seems reasonable to expect that in our case the primary drop in anion–cation energy comes from the more numerous and exposed phenyl groups of the phosphonium core as opposed to the phenoxyfluorophenyl appendage. At the far left, the anion-triphenylphosphonium energy is further broken down at the atomic scale and found to be mostly a result of changes in the anion's interaction with the *meta* and *para* hydrogens of the triphenylphosphonium core, ANI–H3 and ANI–H4, respectively. Thus the primary cause of the drop in enthalpy, and hence the drop in melting point, is a change in the interaction energy between the anions and the distal hydrogens of the triphenylphosphonium core. Note that these interactions, on their own, are largely favourable. In the next section we examine the change in structure that accompanies these energetic changes.

3.3.2 IL Structure

Site–site radial distribution functions, $g(r)$, were constructed between the oxygen atoms of bistriflimide and the *para*–oriented hydrogen atoms of the triphenylphosphonium core (see Figure 4). These functions give the probability of finding the two atoms a distance r from one another, relative to that of a completely random distribution at an equivalent density. Figure 4 shows $g(r)$ of

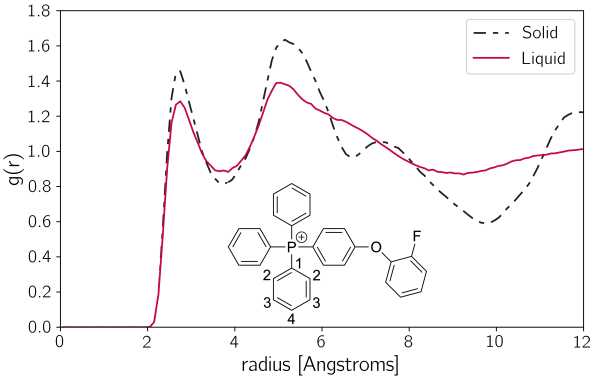

(a)

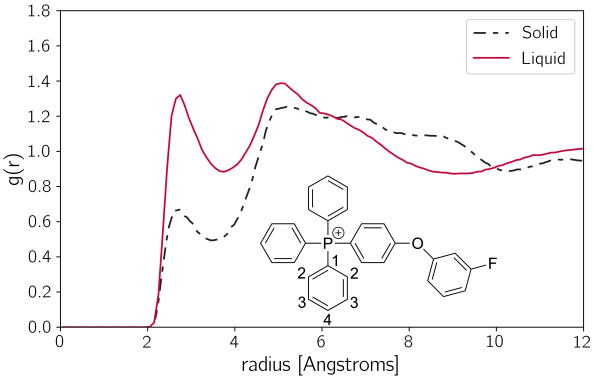

(b)

Fig. 4 Site-Site distribution functions between the *para*–linked hydrogens, H4, of the triphenylphosphonium core and the oxygen atoms of bistriflimide for (a) **6** and (b) **7**.

Table 2 Calculated enthalpies of fusion obtained from MD alongside thermodynamic properties obtained from DSC.

Compound	H^S (kJ/mol)	H^L (kJ/mol)	ΔH_{fus} (kJ/mol)	ΔH_{fus}^{exp} (kJ/mol)	ΔS_{fus}^{exp} (J/mol-K)	T_m^{exp} (K)
6	736.4	942.8	206.4	34.1	87.0	391.9
7	530.1	731.6	201.5	29.3	85.9	341.3
6 $\longrightarrow$ **7**	-206.3	-211.2	-4.9	-4.8	-1.1	-50.6

Table 3 Breakdown of the calculated changes in the thermodynamic properties, given in kJ/mol, between **6** and **7**. Abbreviations refer to the (ANI) anion, (CAT) cation, (TRI) triphenylphosphonium core, (POP) the phenoxyphenyl appendage, and (TOT) the total. Numbering of the atoms in the triphenylphonium core are given in the insets of Figure 4.

Finest		Very-Fine		Fine		Coarse		Coarsest	
Type	$\Delta\Delta U_{pair}$	Type	$\Delta\Delta U_{pair}$	Type	$\Delta\Delta U_{pair}$	Type	$\Delta\Delta U_{pair}$	Type	$\Delta\Delta H_{fus}$
CAT-CAT	-2.5	**CAT-CAT**	-2.5	**CAT-CAT**	-2.5				
ANI-P	-1.3								
ANI-C1	-2.1								
ANI-C2	0.0								
ANI-H2	2.1	**ANI-TRI**	-15.1	**ANI-CAT**	-9.6	**TOT**	-6.7	**TOT**	-4.9
ANI-C3	4.6								
ANI-H3	-9.2								
ANI-C4	-0.4								
ANI-H4	-8.8								
ANI-POP	5.4	**ANI-POP**	5.4						
ANI-ANI	5.4	**ANI-ANI**	5.4	**ANI-ANI**	5.4				

both the crystalline and liquid states for (top) **6** and (bottom) **7**. Each function has a first peak at 2.5 Å corresponding to the near contact of the oxygens with the *para*–oriented hydrogens. The g(r) of the liquid state for both compounds (solid red lines) are nearly indistinguishable. Interestingly, the major difference between these two compounds lies in the crystalline state. IL **6** has a crystal structure that is remarkably similar to its liquid state. On melting, there is a slight weakening of the first two peaks as expected. The $g(r)$ of the crystal state for compound **7**, conversely, has a very weak first peak, indicating a lack of oxygen near the *para*–oriented hydrogens in this state. Upon melting, there is a substantial strengthening of the peak, indicating increased contacts between these two atom types. Since these interactions are strong and favourable this would significantly decrease ΔU_{pair}, which would lower ΔH_{fus}, and ultimately lower the melting point.

From Figure 4 it is apparent that the major difference between **6** and **7** lies in their crystal structures and specifically, the lack of oxygen to *para*–oriented hydrogen contacts in the latter. In the next section we take a closer look at these structures to determine how this relates to the significant difference in ΔH_{fus} between these two compounds.

3.3.3 Crystal Structure

The (001) face of the orthorhombic **6** crystal is shown in Figure 5(a). All of the cations and anions in this figure are shown as blue and red lines, respectively. Since it was determined in the above sections that the most influential change in the system occurs between the anions and the distal hydrogen atoms of the triphenylphosphonium core, the figure also highlights one of the central cations along with all of the anions coordinated with the core. Figure 5(c) displays a closeup of these highlighted molecules and has a total of seven anions that are in coordination.

The (001) face of the monoclinic **7** crystal is shown in Figure 5(c). The cations and anions in this figure are colored as in the previous figure. Here it is evident that the anions form into distinct linear domains perpendicular to the (001) face. Again, one of the cations within the lattice has been highlighted along with anions and one of the neighbouring cations that are coordinated with the triphenylphosphonium core. Figure 5(d) displays a closeup of these highlighted molecules and shows only six coordinated anions, as opposed to the seven seen for the other salt. Furthermore, one of the core phenyl groups is obstructed by a neighbouring cation, preventing anion coordination at that site. This difference in the numbers of cations is also reflected in the pair distribution functions of the solid states, dashed lines in Figure 4. Cation **6**, which has one more coordinated anion than **7** in the crystalline state, has a significantly higher first peak around 3 Å. This strongly suggests that the partial blocking of one of the phenyl groups in the core of the **7** by a neighbouring cation in the cationic domain raises the free energy of the crystalline state. Upon melting, the phenyl group becomes unobstructed, providing access to an additional anion for coordination This leads to a favourable energetic change and a lower ΔH_{fus} for **7** compared with **6**, which would drive down the melting point. Cation **6**, conversely, already has seven coordinated anions and upon melting it gains no additional anions for coordination with the phenyl groups of the cation core.

Figure 5(e) shows selected molecules in the cationic domain of the **7** crystal. Some of the cations associate into chains directed perpendicular to the face of Figure 5(c). Specifically the fluo-

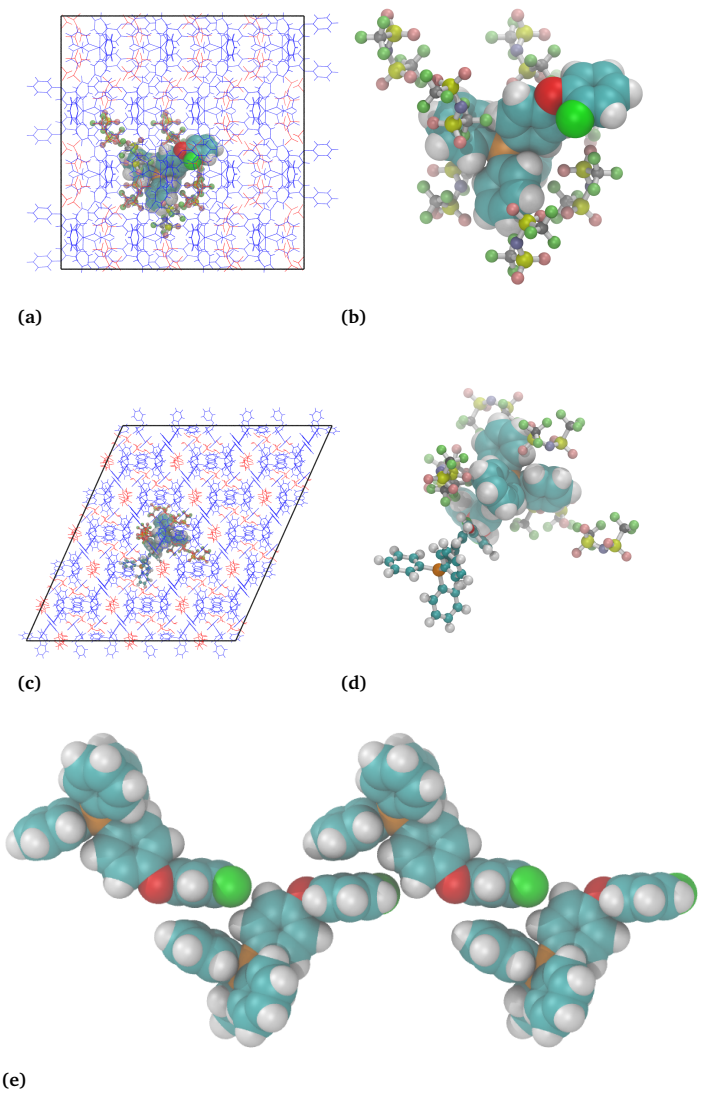

Fig. 5 Crystalline structures of (a) **6** and (c) **7** highlighting a single cation with anions near the triphenylphosphonium base. Cations are shown as blue lines and anions as red lines. Closeup views of (b) the highlighted cation in (a) with seven anions in proximity to the triphenylphosphonium core and (d) the highlighted cation in (c) with only six anions and another cation in proximity to the triphenylphosphonium core. (e) A chain of phenoxyfluorophenyl present in the crystal of **7**.

rine atoms of each cation, representing the most negative site of the cation, are in near contact with the phosphonium atoms, representing the most positive site of the cation, of a neighbouring cation. The line between these two atoms in the same cation roughly corresponds to the dipole moment of the cation, and Figure 5(e) shows near alignment end–on–end of these neighbouring cations. This provides visual evidence that a strong dipole moment can lead directly to cationic clustering in the crystalline structure.

3.4 Additional Crystal Structures

Two additional crystal structures, those of cation **4** and **5** were obtained from single crystal X-ray diffraction. Unfortunately, we were unsuccessful in growing crystals of additional isomers of these compounds, which would have been useful for a direct energetic comparison. Nonetheless, we now analyze the arrangements of the cations and anions in these structures to provide any base of similarity with the compounds described in detail above.

The crystal structure of cation **4** had a fixed position of the backbone atoms but with a four–fold disorder of fluorine among each of the phenyl rings. One of these possibilities is displayed in Figure 6. Similar to cation **7** there is a crystallographic plane

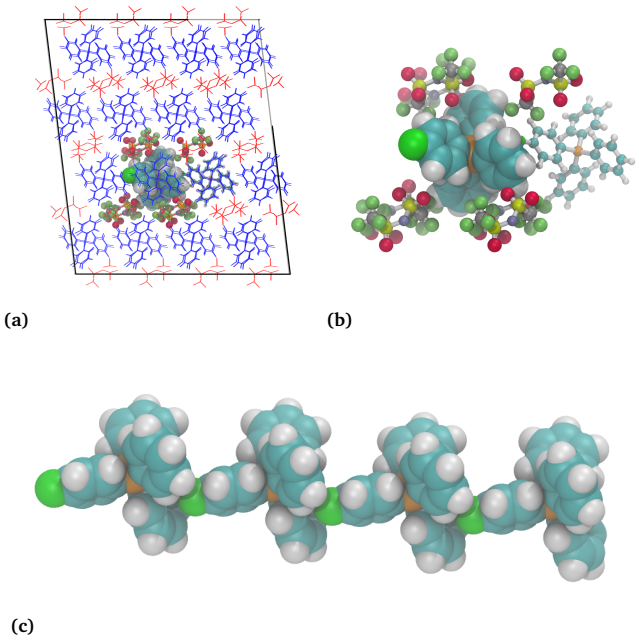

Fig. 6 The crystalline structure of **4** highlighting a single cation with anions near the triphenylphosphonium base. Cations are shown as blue lines and anions as red lines. (b) Closeup view of the highlighted cation with anions and another cation in proximity to the triphenylphosphonium core. (c) A chain of phenoxyphenyl present in the crystal of **4**.

that shows a clear separation of the cations and anions, blue and red in Figure 6(a), respectively. Notice the linear domains of each, visible horizontally in the figure, but also present perpendicular to the plane of the page. Naturally, this means that the cations are in close contact with other anions. Figure 6(b) shows a closeup of one such cation with the neighbouring cations

and anions highlighted. As with compound **7** shown earlier, this structure also has sides of the triphenylphosphonium core that are obstructed by neighbouring cations. Figure 6(c) shows a chain of neighbouring cations that extends throughout the crystalline structures. Here, the fluorophenyl group of each cation is nestled in the triphenylphosphonium core of a neighbouring cation. Thus the dipole moment created by the position of the fluorine atom on the phenyl group induces a dipole orientation between neighbouring cations. We again note that the single crystal x-ray structure showed four–fold disorder in the directionality of the fluorine atom however, two of those possible directions leave the fluorine nestled in the triphenylphosphonium core of a neighbouring cation. We presume that beyond the formation of these linear domains, this compound is likely to form zig–zag patterns throughout the structure that preserve the cation–cation directionality of the dipole moments.

The crystal structure of cation **5** is displayed in Figure 7(a). This crystal also has a crystallographic plane providing an unobstructed view of the clear separation of anion and cation domains, similar to that of Figures 5(c) and 6(a). Figure 7(b,c) shows that this cation forms extended domains of cations, having the phenoxyphenyl group nestled in the triphenylphosphonium core of neighbouring cations. In doing so, anions are partially blocked from favourable interactions with the triphenylphosphonium core. It is presumed that, like **7** discussed above, the melting of this crystal allows for recovery of these favourable interactions, leading to a larger overall drop in ΔH_{fus}. Together, this would serve to lower the melting point.

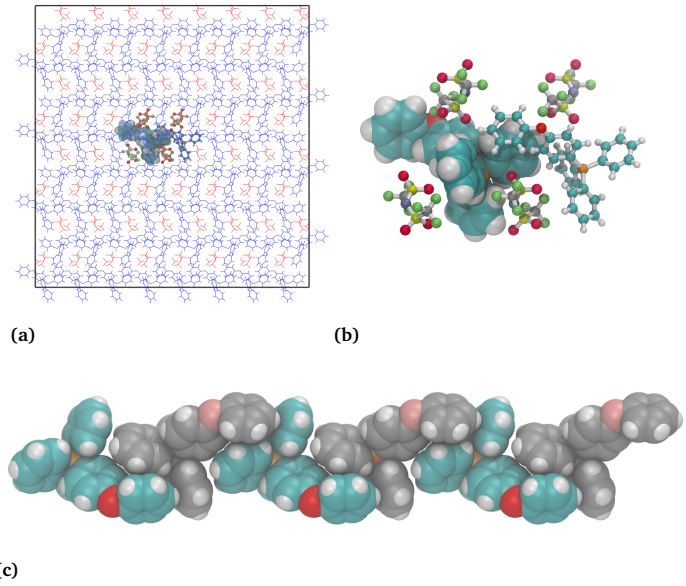

Fig. 7 The crystalline structure of **5** highlighting a single cation with anions near the triphenylphosphonium base. Cations are shown as blue lines and anions as red lines. (b) Closeup view of the highlighted cation with anions and another cation in proximity to the triphenylphosphonium core. (c) A chain of phenoxyphenyl present in the crystal of **5**. Successive cations have been given a different color scheme to distinguish individual cations.

3.5 Exceptions to the Rule

The plot of the change in the dipole moment versus the change in the melting point (Figure 3) showed that there is a general decrease in the melting point with increased dipole moment. There are however, three exceptions to this rule: cations **6**, **21**, and **14**, which are now discussed in more detail. The behaviour of cation **6** was discussed above, however we note again that although the dipole moment of this cation is greater than that of the parent cation, **5**, the fluorine atom at the *ortho* position of the phenoxyphenyl group is tucked away. Thus cation **6** cannot form extended dipole-dipole oriented chains as readily as cations **4** and **7** discussed in detail above. Therefore, it is believed that the dipole-dipole interaction is not sufficient for **6** to induce crystallization in a cation/anion separated state, like many of the others shown above. It is presumed to crystallize in a similar state as the parent compound.

Similar to cation **6**, cation **21** also has a tucked electronegative atom at the *ortho* position, however without the bulky triphenylphosphonium core, this position is significantly more exposed. Cation **21**, in fact, has a lower melting point than its parent compound, however its dipole moment is lower than this comparator. The electronegative fluorine's positioning near the positive imidazolium ring causes a slight reduction in the overall dipole moment.

Cation **14** is also an exception to the general trend of decreased melting point with increased dipole moment. This cation is quite different from the others in that each of its three fluorophenyl are free to rotate. Because the fluorine atoms are at the *meta* position a concerted rotation of the phenyl groups will either draw the electronegative atoms closer to or further from the core. Since these three groups are free to rotate independently and there is little to no correlation between their orientations, the net effect is a fluctuating dipole moment. These fluctuations are likely to preclude the formation of cation chains like those shown earlier. We presume that the quantum–based calculations, which finds relevant configurations of the cation in a conductor–like environment, may overestimate this compound's dipole moment. Note that this does not occur for cation **15**, which shows a near 70 °C drop in melting point relative to the parent compound. With fluorines in the *para* position, a rotation of the fluorophenyl group will not move the electronegative atoms relative to the phosphonium core. Thus this cation has a fixed dipole moment, one that could potentially align with neighbouring cations, producing a drop in the melting point as discussed above.

4 Conclusions

We performed a systematic study examining the effect on the thermodynamic properties of a modified distribution of the electrostatic potential in a set of ionic liquid cations. ILs based on four different cation classes paired with bistriflimide were synthesized. In each case either a single or multiple hydrogens at specific locations in the parent compound were replaced with fluorine atoms. This changes the distribution of the electrostatic potential of the cation, and the cation's dipole moment as shown by quantum calculations, while minimally affecting the cation sterics. DSC measurements of these compounds showed that, in general, an

increase in the dipole moment of the cation lowers the melting point of these compounds when compared with that of the parent compound.

Collectively, the foregoing data show that the addition of strong, directional interactions in IL cations can drive down the melting point, in agreement with earlier observations for imidazolium-based ILs. We show that this primarily occurs by increasing the free energy of the crystalline state. Strong directional interactions force the cations and anions to arrange into separate domains in the crystal state, a finding that we believe to be of fundamental importance in understanding the relationship between salt melting points and cations structures in ionic liquids in particular, and likely molecular salts in general. If, however, the directional interactions are too strong the compounds were found to form glasses. Finally, we note that the ability of the cation to obstruct favourable cation–anion contacts through the formation of cation chains appears crucial to this behaviour. Future studies will explore the limits of this principle when applied to different classes of IL anions.

Conflicts of interest

There are no conflicts to declare.

Acknowledgements

Materials, reagents, and the synthetic work were funded through grants by the NSF CHE-1464740. Computational work was funded through the DOE Office of Science (DE-SC0020282) through the Separations and EPSCoR programs and Energy Efficiency and Renewable Energy Advanced Manufacturing Office. We would also like to acknowledge the help of Dr. Matthias Zeller of the Department of Chemistry at Purdue University for the acquisition of the single-crystal X-ray structures. Additionally, the simulations were made possible through a grant of high performance computing resources and technical support from the Alabama Supercomputing Authority.

Notes and references

1 B. D. Rabideau, K. N. West and J. H. Davis, *Chemical communications (Cambridge, England)*, 2018, **54**, 5019–5031.

2 C. G. Cassity, A. Mirjafari, N. Mobarrez, K. J. Strickland, R. A. O'Brien and J. H. Davis, *Chemical communications (Cambridge, England)*, 2013, **49**, 7590–7592.

3 M. D. Ediger and P. Harrowell, *The Journal of Chemical Physics*, 2012, **137**, 080901.

4 O. Lebel, T. Maris, M.-E. Perron, E. Demers and J. D. Wuest, *Journal Of The American Chemical Society*, 2006, **128**, 10372–10373.

5 T. Niemann, D. Zaitsau, A. Strate, A. Villinger and R. Ludwig, *Scientific reports*, 2018, **8**, 14753.

6 T. Niemann, P. Stange, A. Strate and R. Ludwig, *Chemphyschem : a European journal of chemical physics and physical chemistry*, 2018, **19**, 1691–1695.

7 L. Chen and V. S. Bryantsev, *Physical Chemistry Chemical Physics*, 2017, **19**, 4114–4124.

8 I. L. Martin, E. Burello, P. N. Davey, K. R. Seddon and G. Rothenberg, *Chemphyschem : a European journal of chemical physics and physical chemistry*, 2007, **8**, 690–695.

9 M. Bujak, *Acta crystallographica Section B, Structural science, crystal engineering and materials*, 2018, **74**, 458–466.

10 N. V. Plechkova and K. R. Seddon, *Chemical Society Reviews*, 2007, **37**, 123–150.

11 M. K. Mishra, S. P. Kelley, J. L. Shamshina, H. Choudhary and R. D. Rogers, *Crystal Growth & Design*, 2018, **18**, 597–601.

12 S. M. Murray, R. A. O'Brien, K. M. Mattson, C. Ceccarelli, R. E. Sykora, K. N. West and J. H. Davis, *Angewandte Chemie International Edition*, 2010, **49**, 2755–2758.

13 R. A. O'Brien, A. Mirjafari, K. M. Mattson, S. M. Murray, N. Mobarrez, E. A. Salter, A. Wierzbicki, J. James H Davis and K. N. West, *The Journal of Physical Chemistry B*, 2014, **118**, 10232–10239.

14 R. A. O'Brien, M. S. Zayas, S. T. Nestor, J. C. Gaitor, L. M. Paul, F. A. Edhegard, S. Minkowicz, R. E. Sykora, Y. Sheng, S. F. Michael, S. Isern and A. Mirjafari, *New Journal Of Chemistry*, 2016, **40**, 7795–7803.

15 M.-L. Kwan, A. Mirjafari, J. R. McCabe, R. A. O'Brien, D. F. Essi IV, L. Baum, K. N. West and J. H. Davis Jr., *Tetrahedron Letters*, 2013, **54**, 12–14.

16 A. Mirjafari, S. M. Murray, R. A. O'Brien, A. C. Stenson, K. N. West and J. H. Davis, *Chemical Communications*, 2012, **48**, 7522.

17 S. Ahrens, A. Peritz and T. Strassner, *Angewandte Chemie International Edition*, 2009, **48**, 7908–7910.

18 P. Bonhôte, A.-P. Dias, N. Papageorgiou, K. Kalyanasundaram and M. Grätzel, *Inorganic chemistry*, 1996, **35**, 1168–1178.

19 A. J. McLean, M. J. Muldoon, C. M. Gordon and I. R. Dunkin, *Chemical communications (Cambridge, England)*, 2002, 1880–1881.

20 O. Okoturo and T. VanderNoot, *Journal of Electroanalytical Chemistry*, 2004, **568**, 167 – 181.

21 P. A. Hunt, *The Journal of Physical Chemistry B*, 2007, **111**, 4844–4853.

22 T. Endo, T. Kato and K. Nishikawa, *The Journal of Physical Chemistry B*, 2010, **114**, 9201–9208.

23 K. Noack, P. S. Schulz, N. Paape, J. Kiefer, P. Wasserscheid and A. Leipertz, *Physical Chemistry Chemical Physics*, 2010, **12**, 14153–14161.

24 K. Fumino, A. Wulf and R. Ludwig, *Angewandte Chemie International Edition*, 2008, **47**, 8731–8734.

25 T. Peppel, C. Roth, K. Fumino, D. Paschek, M. Köckerling and R. Ludwig, *Angewandte Chemie International Edition*, 2011, **50**, 6661–6665.

26 C. A. Cassity, B. Siu, M. Soltani, J. L. McGeehee, K. J. Strickland, M. Vo, E. A. Salter, A. C. Stenson, A. Wierzbicki, K. N. West, B. D. Rabideau and J. H. Davis, *Physical Chemistry Chemical Physics*, 2017, **19**, 31560–31571.

27 N. A. Meanwell, *Journal of medicinal chemistry*, 2018, **61**, 5822–5880.

28 A. C. Stenson, K. N. West, W. M. Reichert, P. Klomkaew, C. G. Cassity, B. M. Dobyns, B. Siu and J. H. J. Davis, *Chemical Communications*, 2015, **51**, 15914–15916.

29 B. Siu, C. G. Cassity, A. Benchea, T. Hamby, J. Hendrich, K. J. Strickland, A. Wierzbicki, R. E. Sykora, E. A. Salter, R. A. O'Brien, K. N. West and J. H. Davis, *RSC Advances*, 2017, **7**, 7623–7630.

30 A. Benchea, B. Siu, M. Soltani, J. H. McCants, E. A. Salter, A. Wierzbicki, K. N. West and J. James H Davis, *New Journal Of Chemistry*, 2017, **41**, 7844–7848.

31 M. Soltani, B. Siu, E. A. Salter, A. Wierzbicki, K. N. West and J. H. Davis Jr., *Tetrahedron Letters*, 2017, **58**, 4628–4631.

32 M. J. Frisch, G. W. Trucks, H. B. Schlegel, G. E. Scuseria, M. A. Robb, J. R. Cheeseman, G. Scalmani, V. Barone, G. A. Petersson, H. Nakatsuji, X. Li, M. Caricato, A. V. Marenich, J. Bloino, B. G. Janesko, R. Gomperts, B. Mennucci, H. P. Hratchian, J. V. Ortiz, A. F. Izmaylov, J. L. Sonnenberg, Williams, F. Ding, F. Lipparini, F. Egidi, J. Goings, B. Peng, A. Petrone, T. Henderson, D. Ranasinghe, V. G. Zakrzewski, J. Gao, N. Rega, G. Zheng, W. Liang, M. Hada, M. Ehara, K. Toyota, R. Fukuda, J. Hasegawa, M. Ishida, T. Nakajima, Y. Honda, O. Kitao, H. Nakai, T. Vreven, K. Throssell, J. A. Montgomery Jr, J. E. Peralta, F. Ogliaro, M. J. Bearpark, J. J. Heyd, E. N. Brothers, K. N. Kudin, V. N. Staroverov, T. A. Keith, R. Kobayashi, J. Normand, K. Raghavachari, A. P. Rendell, J. C. Burant, S. S. Iyengar, J. Tomasi, M. Cossi, J. M. Millam, M. Klene, C. Adamo, R. Cammi, J. W. Ochterski, R. L. Martin, K. Morokuma, O. Farkas, J. B. Foresman and D. J. Fox, 2016.

33 J. Wang, R. M. Wolf, J. W. Caldwell, P. A. Kollman and D. A. Case, *Journal Of Computational Chemistry*, 2004, **25**, 1157–1174.

34 T. Fox and P. Kollman, *The Journal of Physical Chemistry B*, 1998, **102**, 8070–8079.

35 K. G. Sprenger, V. W. Jaeger and J. Pfaendtner, *The Journal of Physical Chemistry B*, 2015.

36 S. Plimpton, *Journal Of Computational Physics*, 1995, **117**, 1–19.

37 R. W. Hockney and J. W. Eastwood, *Computer Simulation Using Particles*, CRC Press, 1989.

38 L. Martinez, R. Andrade, E. G. Birgin and J. M. Martinez, *Journal Of Computational Chemistry*, 2009, **30**, 2157–2164.

39 G. S. Larsen, P. Lin, K. E. Hart and C. M. Colina, *Macromolecules*, 2011, **44**, 6944–6951.

40 Y. WANG, B. Li, A. Laaksonen and J. Yuan, *Chemphyschem : a European journal of chemical physics and physical chemistry*, 2020, cphc.201901206.